Coupling initial hydrogel microenvironments with mesenchymal stem cell remodeling to define a dynamic hematopoietic stem cell niche

Aidan E. Gilchrist[1], Sunho Lee[2], Yuhang Hu[2], Brendan A.C. Harley[3,4]

[1] Dept. of Materials Science and Engineering
[2] Dept. of Mechanical Science and Engineering
[3] Dept. of Chemical and Biomolecular Engineering
[4] Carl R. Woese Institute for Genomic Biology

University of Illinois at Urbana-Champaign
Urbana, IL 61801

Corresponding Author:
B.A.C. Harley
Dept. of Chemical and Biomolecular Engineering
Carl R. Woese Institute for Genomic Biology
University of Illinois at Urbana-Champaign
110 Roger Adams Laboratory
600 S. Mathews Ave.
Urbana, IL 61801
Phone: (217) 244-7112
Fax: (217) 333-5052
e-mail: bharley@illinois.edu

ABSTRACT

Hematopoietic stem cells (HSCs) reside in the bone marrow within discrete niches defined by a complex milieu of external signals including biophysical cues, bound and diffusible biomolecules, and heterotypic cell-cell interactions. Recent studies have shown the importance of autocrine-mediated feedback of cell-secreted signals and the interplay between matrix architecture and biochemical diffusion on hematopoietic stem cell activity. Autocrine and paracrine signaling from HSCs and niche-associated mesenchymal stromal cells (MSCs) have both been suggested to support HSC maintenance *in vivo* and *in vitro*. Here we report the development of a library of methacrylamide-functionalized gelatin (GelMA) hydrogels to explore the balance between autocrine feedback and paracrine signals from co-encapsulated murine bone marrow MSCs on murine HSCs. The use of a degradable GelMA hydrogel enables the possibility ~~for~~ significant MSC-mediated remodeling, yielding dynamic shifts in the matrix environment surrounding HSCs. We identify a combination of an initially low-diffusivity (autocrine dominated) hydrogel and a 1:1 HSCP:MSC seeding ratio as conducive to enhanced HSC population maintenance. Further, gene expression and serial mechanical testing data suggests that MSC-mediated matrix remodeling is significant for the long-term HSC culture, reducing HSC autocrine feedback and potentially enhancing MSC-mediated paracrine signaling over 7-day culture *in vitro*. This work demonstrates the design of an HSC culture system that couples initial hydrogel properties, MSC co-culture, and concepts of dynamic reciprocity mediated by MSC remodeling to achieve enhanced HSC maintenance.

Keywords:

hematopoietic stem cell, hydrogel, mesenchymal stromal cell, remodeling, differentiation

1. Introduction

Hematopoietic stem cells (HSCs) possess the capacity for self-renewal and can repopulate the body's entire complement of blood and immune cells through a highly regulated differentiation hierarchy [1-4]. Following development, HSCs lodge primarily in the bone marrow in unique tissue microenvironments termed *niches*. The niche provides a constellation of extrinsic signals in the form of biophysical cues, biomolecular gradients, and co-inhabiting niche cells that together promote quiescence, self-renewal, and lineage specification of HSCs [5-10]. Due to their multilineage potential, HSC transplants (HSCTs) are a valuable clinical tool for the treatment of a range of blood and immune disorders [11]. However, clinical use of HSCTs has been hindered by disruption of the native niche *in vivo*, resulting in a loss of normal hemostasis during transplantation and a loss in HSC potential [12]. The impact of HSC transplants may be increased if *in vitro* tools were available to promote HSC homeostasis, leading to potentially improved expansion or preconditioning to facilitate better homing and engraftment of transplanted donor HSCs. A potential route to such a clinically relevant transplant tool is the development of biomaterial culture systems that are able to provide the correct sequence of signals to enhance HSC expansion *in vitro*. While exact replication of the native niche is prohibitively complex due to its transient nature, heterogeneity, and coupling of external factors, insight from the native niche can inform the development of a synthetic culture platform that mediates HSC response [13].

Knockout (depletion) and proximity principal (localization) models, both *in vivo* and *in vitro*, have been used to elucidate a range of triggers present in the microenvironment that maintain HSC hematopoietic activity [14]. More recently, tissue engineering approaches have begun to identify critical biomaterial design parameters inspired by native niche signals for *ex vivo* HSC culture. For example, the native bone marrow niche presents complex patterns of ligands such as laminins and fibronectin [15, 16] as well as an effective Young's modulus ranging from 0.25 to

24.7 kPa [17]. Matrix biophysical cues such as elasticity and substrate stiffness can significantly influence HSC expansion and migration, with elastic substrates functionalized with fibronectin shown to induce *ex vivo* expansion of HSC progenitor populations [1-3, 18, 19]. Beyond the extracellular matrix features of the niche, HSCs are surrounded by cellular components within the bone marrow. Niche-associated cells can exert an influence on HSC activity via cadherin interactions, as well as secreted biomolecular factors [20, 21]. In the native niche, the structure of the ECM modulates biotransport of secreted factors via presentation of transient binding motifs (e.g. proteoglycans) and via steric hindrance to diffusive and advective mass transport [22-25]. Engineering approaches have explored the use of cadherin signaling to influence hematopoietic cell activity [26] and modulate autocrine feedback of monolithic HSC cultures [27]. Additionally, biomaterial design of an artificial niche offers the opportunity to regulate the transport of biomolecular signals in heterotypic cultures, and engineer HSC-generated autocrine feedback and niche cell paracrine signals. In a tight matrix, with a small mesh size and low diffusivity, HSCs may experience a small radius of communication, as cell-cell communication is hindered by steric and electrostatic interactions with the matrix, enforcing a mostly autocrine feedback-rich environment. Alternatively, in a loose matrix, with a large mesh size, HSCs have a larger radius of communication, allowing for possible paracrine signaling. Recently, *Pompe et al*. demonstrated that the culture of HSCs microcavities as either single HSCs or pairs led to differential signaling, with autocrine feedback dominating quiescent HSC maintenance [28]. Replicating aspects of this concept in a three-dimensional collagen hydrogel system, we recently showed the ability to maintain early progenitor HSC populations in autocrine-dominated environments with low diffusivity [29].

Mesenchymal stromal cells (MSCs) are found throughout the marrow cavity and are believed to play a pivotal role in HSC homeostasis. Predominantly co-localized with HSCs, they influence hematopoietic activity in the perivascular regions and the central marrow [30, 31]. Here,

paracrine signaling from proximal MSCs mediate HSC activation and quiescence through production of factors such as CXCL12 [32], IL-6 [33, 34], and TPO [35] that regulate HSC activity via diffusive signaling and direct cell-cell contact [6, 28, 31, 36-39]. While co-cultures of HSCs and MSCs within a hydrogel matrix offer the opportunity to identify heterotypic cultures that support HSC quiescence or self-renewal, such studies are significantly complicated by the dynamic reciprocity between inhabiting cells and the surrounding matrix. Notably, while the matrix can impart cues to inhabiting cells, many cells are also equipped to remodel the matrix [40, 41], leading to a dynamic feedback loop. Specifically, MSCs play a significant role in the dynamic remodeling of the ECM through deposition of proteins and enzymatically cleavable motifs within the matrix [42, 43]. Additionally, through adhesion contacts, MSCs create strain

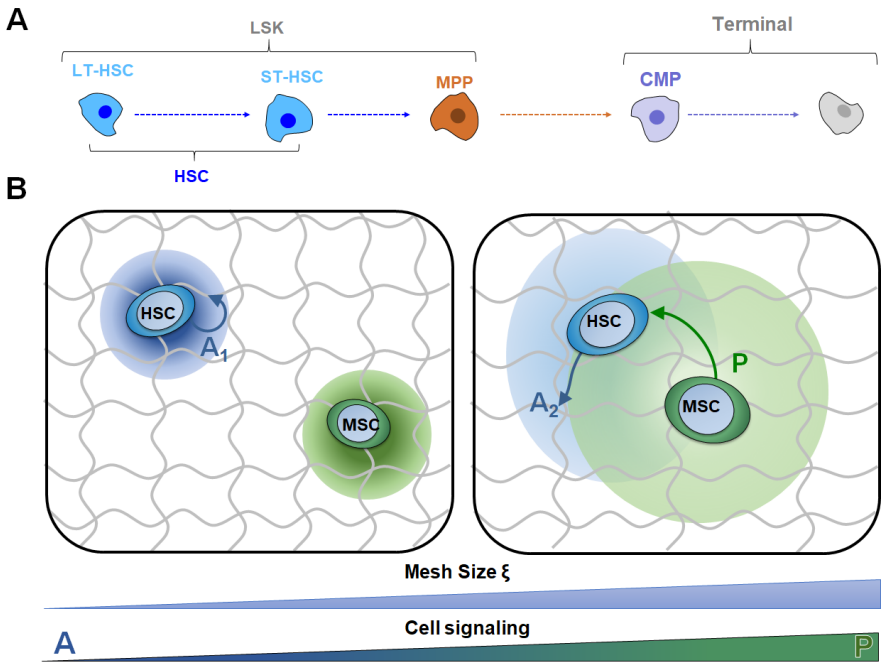

Figure 1. Hematopoietic cell-cell interactions in a dynamic biomaterial landscape. **A)** Hematopoietic lineage hierarchy. Long-term repopulating HSCs and Short-term repopulating HSCs are grouped as a singular HSC population. HSCs and Multipotent Progenitors comprise the HSC progenitor, HSCPs, population. Common Myeloid Progenitors and Lin+ cells make up the Terminal cell population. **B)** Autocrine and paracrine signaling can be tuned by adjusting seeding density and altering biotransport properties. In an HSC-only culture, an increase in mesh size leads to a diffusive regime that increases paracrine signaling. In an HSC-MSC co-culture, small mesh constrains secreted biomolecules and leads to a mostly autocrine signaling. However, as mesh size is increased, autocrine feedback is reduced and paracrine signaling begins to dominate cell-cell interactions

gradients and deformation in the local environment, the so-called peri-cellular region [43]. And as the matrix is altered, the domains of autocrine feedback and paracrine signaling will themselves be affected, shifting the biomaterial landscape and the kinetics of cell-cell and cell-matrix interactions. Exactly how the dynamic reciprocity between cells and matrix influences HSC behavior remains largely unexplored, and offers an exciting opportunity for biomaterial development and characterization.

The objective of this study was to examine the effect of MSC co-culture on HSC differentiation patterns within a three-dimensional gelatin hydrogel under development as a HSC niche analog. Here, we examined not only the influence of initial hydrogel properties on HSC activity but also the integrated influence of MSC-mediated paracrine signals and matrix remodeling on HSC lineage regulation. We created a library of photopolymerized methacrylamide-functionalized gelatin (GelMA) hydrogels with defined initial mechanical and biotransport properties that spanned a range of marrow-inspired properties. Murine HSCs were cultured in a homologous series of GelMA hydrogels in the presence or absence of increasing concentrations of murine bone marrow derived MSCs (**Fig. 1**). We subsequently examined the activation of remodeling associated genes in MSCs, the extent of GelMA matrix remodeling via mechanical analyses, and the influence of heterotypic MSC-HSC culture on HSC self-renewal and myeloid lineage specification.

2. Materials and Methods

2.1 Material characterization

2.1.1 GelMA synthesis and hydrogel fabrication

Porcine Type A gelatin (Sigma, St. Louis, MO) was functionalized along its backbone with pendulant methacrylamide groups following a previously described protocol [44, 45]. In brief, methacrylate anhydride (MA) was added dropwise to a solution of gelatin in PBS before

quenching in excess PBS, purification via dialysis, and lyophilization. The ratio of gelatin to MA was tuned to control the degree of functionalization (35%, 50%, 85% DOF; quantified by H^1 NMR) [45]. Methacrylamide-functionalized gelatin (GelMA) hydrogel variants were subsequently formed from 20μL of GelMA precursor suspension mixed with a lithium acylphosphinate (LAP) photoinitiator (PI) in circular Teflon molds (5mm dia.) exposed to 7.14 mW/cm^2 UV light for 30 seconds. After crosslinking, hydrogels were immediately hydrated in PBS [46, 47].

2.1.2 Determination of poroelastic properties

A library of 18 acellular hydrogels were fabricated from 35, 50, and 85% DOF GelMA at 4, 5, and 7.5% (w/v) GelMA, with 0.05 or 0.1% (w/v) PI. The Young's modulus of the complete library of hydrogels was determined using an Instron 5943 mechanical tester in unconfined compression (Instron, Norwood, MA). Briefly, a preload was applied to each sample at a rate of 0.05 N/min until a load of 0.005 N was reached. Then compression at a rate of 0.1mm/min was applied until 20% compression was reached. The Young's modulus was taken as the slope of the linear fit applied to 10% of the compressive stress vs. compressive strain data using Origin Statistical Software (Northampton, MA) [48, 49]. An offset of 0 or 5% strain was applied prior to linear fit analysis to confirm that the compression platen was completely in contact with the hydrogel surface. The elastic moduli of cellular hydrogels containing 1:1 or 1:10 MSCs ($1x10^5$ or $1x10^6$ MSCs/mL; experimental description below) were traced over seven days in culture, using the same compression protocol. After mechanical analysis, MSC-seeded hydrogels were immediately put on dry ice and stored at -80°C for subsequent gene expression analyses.

Stress-relaxation indentation tests were performed on acellular hydrogels specimens using MFP-3D AFM (Asylum Research, Goleta, CA), with a 4.5μm spherical tip (Novascan, Ames, IA). The generated force curve was used to extract out the shear modulus and diffusion coefficient of water. Specimens were indented to 0.5, 1, or 2μm as rapidly as possible to approximate

instantaneous compression, and held for a test time of 5 seconds. This process has been described elsewhere, but in brief, the instantaneous force was normalized to the far-field force and fitted to a finite element analysis formula by modulating the characteristic time and material properties (shear modulus, diffusion) [50-53].

2.1.3 Mesh size estimate

The mesh size of the hydrogel library was determined from the swelling ratios of the hydrogels [54-56]. The mesh size is a function of the volume fraction and the mean-squared end-to-end distance of the polymer chain.

$$(1) \qquad \xi = v_{2s}^{-\frac{1}{3}} * \left(l\left(2\frac{M_c}{M_r}\right)C_n\right)^{\frac{1}{2}}$$

In determining material parameters it was assumed that the gelatin chains were long enough to neglect chain-end effects. It was also assumed that the molecular weight of the repeat unit, M_r, was the averaged molecular weight of the amino acid composition. Amino Acid Analysis was performed at the UC Davis Genome Center with a Hitachi L-8900 (Li-based) analyzer. The mass swelling ratio of a hydrogel is determined by the ratio of the dry to wet weight. The swelling ratio was determined for hydrogels in a relaxed and equilibrium state, immediately following crosslinking or after 24hrs in PBS respectively. At each time, hydrogels were weighed wet, and then weighed again after lyophilization. The mass swelling ratio was then transformed to volumetric swelling ratio following the equation below, and using the solvent density ($\rho_{PBS} = 1.01 g/cm^3$) [57] and polymer density ($\rho_{gelatin} = 1.345 g/cm^3$) [58-60].

$$(2) \qquad Q_v = 1 + \frac{\rho_p}{\rho_s}(Q_m - 1)$$

From this, the volume fraction of polymer is calculated as:

$$(3) \qquad v = \frac{1}{Q_v}$$

The molecular weight between crosslinks, M_c, was estimated by using the well-known Flory-

Rehner equation adapted by Bray and Merrill for use in polymers crosslinked in solvent [55, 61]. The applicability of the modified equation for specific concentration regimes was confirmed by Peppas and Merrill [54]. The M_c is a function of material properties such as the molar weight of the solvent, V_1, the specific volume of the polymer, $\bar{v}$, and the solvent-polymer interaction, X_1, also known as Flory's Chi parameter. It is also a function of the system parameters such as the volume fraction of the polymer in its relaxed state and in the equilibrium state, v_{2r} and v_{2s}, and the number average molecular weight before crosslinking, M_n.

$$(4) \qquad \frac{1}{M_c} = \frac{2}{M_n} - \frac{\frac{\bar{v}}{V_1}\left[\ln(1-v_{2s})+v_{2s}+X_1 v_{2s}^2\right]}{v_{2r}\left[\left(\frac{v_{2s}}{v_{2r}}\right)^{\frac{1}{3}}-\frac{1}{2}\left(\frac{v_{2s}}{v_{2r}}\right)\right]}$$

Flory's characteristic ratio,C_n, is a measure of the ratio of the length of a polymer to the theoretical length of the polymer and is a function of the number of monomers in a chain, n. The characteristic ratio can be approximated by a constant number as the number of monomers goes to infinity, $\lim_{n\to\infty} C_n = C_\infty$. For a stiff chain, this can be approximated using the worm-like or Kratky-Porod persistence model modified for proteins which uses the persistence length, l_p, and the monomer unit length [62, 63]:

$$(5) \qquad C_\infty = 0.95\frac{2l_p}{l}$$

2.2 Hematopoietic stem cell isolation

All work involving primary cell extraction was conducted under approved animal welfare protocols (Institutional Animal Care and Use Committee, University of Illinois at Urbana-Champaign). Primary murine Hematopoietic stem progenitor cells (HSPC) were extracted from the femur and tibia bone marrow of C57BL/6 female mice, age 4 – 8 weeks (Jackson Labs). The bones were gently crushed with pestle and mortar, and washed with PBS + 5%FBS prior to filtration with a 40μm sterile filter [29, 46]. The collected suspension was lysed with ACK lysis buffer (Invitrogen, Carlsbad, CA), and then rinsed with PBS/FBS. Initial HSPC isolation was performed using defined protocols of EasySep™ Mouse Hematopoietic Progenitor Cell

Enrichment Kit and Magnet (#19756, #18000, Stemcell Technologies, CA). A secondary isolation further enriched the HSPC population by collecting the Lin^{-} $Sca\text{-}1^{+}$ $c\text{-}kit^{+}$ (LSK) fraction using BD FACS Aria II flow cytometer. All antibodies were supplied by eBioscience (San Diego, CA), and are as follows: PE-conjugated Sca-1 (1:100 dilution), APC-efluor780-conjugated c-kit (1:100 dilution), and cocktail of FITC-conjugated lineage specific surface markers (CD5, B220, Mac-1, CD8a, Gr-1, and Ter-119) [64-66]. The LSK faction was collect in PBS + 25% FBS on ice and immediately used [19, 29, 46, 67-70].

2.3 Mesenchymal stromal cell isolation

Murine MSCs were isolated from the femur and tibia bones used for HSPC extraction. Following gentle crushing with a pestle and mortar, MSCs were isolated from bone following commercially available defined protocols of MesenCult™ Proliferation Kit with MesenPure™ (#05512 Stemcell Technologies, CA). The MSCs were cultured in one T25 flask per mouse, and allowed to expand for two weeks prior to collection (zero passage), with a half-media change after one week. Non-adherent cells were washed away and only the adherent cells were collected after trypsinization with Gibco TrypLE (ThermoFisher Scientific, Waltham, MA). Cells were collected on ice and immediately used.

2.4 Hematopoietic stem cell culture in GelMA hydrogel in the presence of MSCs

Single culture HSCPs were encapsulated in GelMA hydrogels at a density of $1x10^5$ HSCPs/mL. Similarly, co-cultures of HSCPs and MSCs were encapsulated at a ratio of 1:1 or 1:10 HSCPs to MSC, keeping a constant density of $1x10^5$ HSCPs/mL. HSCP or MSCs in a suspension of HSC media were added to the hydrogel precursor solution at the desired seeding density of $1x10^5$ HSPCs/mL and $1x10^5$ or $1x10^6$ MSCs/mL, while maintaining the concentration of GelMA. Upon crosslinking, each hydrogel-cell construct was placed into an individual well of a 48-well plate, and cultured at 37°C for 7 days in 300µL StemSpan™ SFEM (#09650 Stemcell Technologies)

supplemented with 100 ng/mL SCF (Peprotech) and 0.1% Pen Strep (Gibco), with media changes every 2 days [19].

2.5. Analysis of HSC differentiation patterns

Differentiation patterns of HSPCs were analyzed via Fluorescence-Assisted Cytometry (FACs), using a BD LSR Fortessa (BD Biosciensces, San Jose, CA). Cell seeded hydrogels were degraded with 100 Units of Collagenase Type IV (Worthington Biochemical, Lakewood, NJ) for 20 minutes at 37°C, and gently mixed via pipetting every five minutes. The reaction was quenched, and the cells were re-suspended in 100μL PBS and 5% FBS and then stained with a cocktail of antibodies (eBioscience, San Diego, CA) to profile HSC lineage specification: eFluor 660 CD34 (1:100 dilution, 90 mins), PerCP-eFluor 710 CD135 (1:100 dilution, 30 mins), eFluor 450 CD16/CD32 (1:200 dilution, 30 mins), APC-eFluor 780 c-Kit (1:800 dilution, 30 mins), PE Sca-1 (1:400 dilution, 30 mins), FITC lineage cocktail (CD5, B220, Mac-1, CD8z, Gr-1, Ter-119, 1:100 dilution, 30 min). Hematopoietic cells were subsequently classified as more primitive Long-Term repopulating HSCs (LT-HSCs: $CD34^{lo}$ $CD135^{lo}$ Lin^{-} $Sca1^{+}$ c-kit^{+}) [69, 71, 72]; differentiated Short-Term repopulating HSCs (ST-HSCs: $CD34^{hi}$ $CD135^{lo}$ LSK) [69, 71, 72]; more differentiated Multipotent progenitors (MPPs: $CD34^{+}$ $CD135^{+}$ LSK) [72, 73], and lineage-specified Common Myeloid Progenitors (CMPs: Lin^{-} c-kit^{+} $Sca1^{-}$ $CD34^{+}$ $CD16/32^{-}$) [73], [65, 74-76]. Individual cell populations are reported as percentages of the total hematopoietic cell population in each culture, with Terminal cells classified as remaining hematopoietic cells that were not part of the LSK fraction. For the purpose of some cell population analyses, LT-HSC and ST-HSC were grouped together as a singular HSC population.

2.6. Analysis of MSC mediated-remodeling profiles

Subsequently, matrix remodeling associated gene expression profiles were examined for MSC-seeded hydrogel specimens via QuantiStudio 7 Flex real-time PCR (Applied Biosystems). Frozen

hydrogels isolated at days 0, 1, 4, and 7 during culture were crushed using a pestle, with mRNA extracted using RNeasy Plant Mini Kit (Qiagen, Germany). mRNA to cDNA was accomplished using the QuantiTect Rev. Transcription kit (Qiagen), and prepped for RT-PCR using PIPETMAX (Gilson, Middleton, WI). The C_T of each gene/sample was performed in duplicate. Results were analyzed using the comparative CT method ($2^{-\Delta\Delta CT}$). Primer specificity and efficiency were validated prior to comparative C_T analysis [77]. Matrix deposition genes examined were collagen, type I, alpha 1 (Col1a1), and tissue inhibitors of metalloprotease TIMP-1, TIMP-2, and TIMP-3. Matrix degradation genes were the matrix metalloproteases MMP-2 and MMP-9, also known as Gelatinase-A and Gelatinase-B [78]. Expression of the glyceraldehyde-3-phosphate dehydrogenase (GAPDH) was used for housekeeping. Gene expression was first normalized to the housekeeping gene (GAPDH), and then compared against the gene expression at day 0 of each specific seeding and hydrogel condition (**Fig. S4**). Primer information can be found in **Table S1.**

2.7. Statistics

All statistics were performed on a minimum of 3 replicates. Significance was tested with Origin Statistical Software using 2-way ANOVA, at a significance level of 0.05. Normality of the data was determined using the Shapiro-Wilkes test at significance 0.05 [79], and homoscedasticity (equality of variance) determined using Levene's Test [80]. Post-hoc power analysis was used to confirm the sample size was large enough to maintain a maximum Type I error of α=0.05, and Type II error of β=0.20 [81, 82]. Young's modulus outliers were removed using Dixon's Q-test at significance level 0.05 [83]. Means are reported with their associated standard deviations. In the comparative C_T method of gene expression, the error was propagated throughout the calculations.

3. Results

3.1. Poroelastic characterization of GelMA hydrogels

The Young's modulus (E) of the complete library of GelMA hydrogels spanned a range of marrow mimetic values (2.67±1.39 to 32.23±10.7kPa), and showed strong dependence on GelMA wt% and, to a lesser extent, degree of functionalization (DOF) of the GelMA (**Fig. S1)**. The different levels of PI (0.05, 0.1%) did not change the modulus drastically, with subsequent analyses here concentrating on the 0.1%PI condition (**Fig. 2A)**. The subset of hydrogels fabricated from 4wt% GelMA demonstrated moduli ranging from 4.67±3.20 (35% DOF) to 7.65±3.90kPa (85% DOF). A midrange subset (5wt% GelMA) showed increased elastic moduli

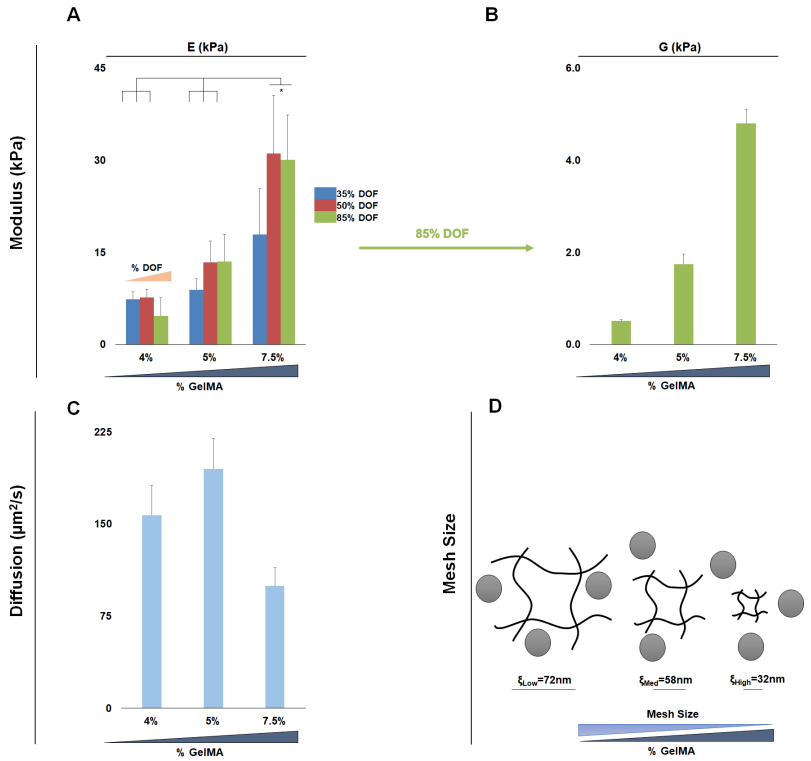

Figure 2. Mechanical characterization of the library of methacrylamide-functionalized hydrogels. (**n=6**). **A)** Young's modulus of 9 hydrogel conditions, keeping the PI constant at 0.1% **B)** Shear modulus data from the *Low*, *Med*, and *High* hydrogel variants used for cell culturing, keeping DOF and PI constant at 85% DOF and 0.1%PI. **C)** Diffusion of water in the *Low*, *Med*, and *High* variants exhibits two regimes, *Low* and *Med* (4, 5% GelMA) have a higher diffusion, whereas *High* (7.5% GelMA) has ~50% reduction in diffusion **D)** Mesh size estimates for the *Low*, *Med*, and *High* variants decreases with increasing GelMA content. There is a trend of *Low* and *Med* exhibiting similar mesh and diffusion, while *High* exhibits a significantly lower regime.

range, from 8.90±1.83 (35% DOF) to 13.54±4.81kPa (85% DOF). The subset fabricated with the highest GelMA concentration (7.5wt%) demonstrated a range of moduli spanning 17.89±10.99 (35% DOF) to 30.06±12.35kPa (35% DOF). We subsequently examined poroelastic properties of the entire library of hydrogels in terms of the shear modulus (G) and the diffusion coefficient of water (D_w). Here, the range of shear moduli spanned 0.36±0.03 to 6.05±0.50kPa (G) while water diffusion ranged from 75.86±11.84 to 211.13±51.84 $\mu m^2/s$ (**Fig. S2** and **S3**).

From this larger library of hydrogels, we selected a subset of three hydrogels (85% DOF, 0.1%PI, and 4, 5, 7.5%GelMA) that spanned a range associated with mechanical properties of the native niche: *Low*, E_{low} = 4.67±3.20; *Med*, E_{med} = 13.54±4.81; *High*, E_{high} = 30.06±12.35kPa (**Fig. 2A)**. This subset also displayed a significant increase in the shear modulus (G_{low} = 0.51±0.03; G_{med} = 1.74±0.22; G_{high} = 4.80±0.3kPa respectively) (**Fig. 2B**). *Low* and *Med* hydrogels displayed similar water diffusion characteristics (157.19±24.45, 195.04±24.66 $\mu m^2/s$) whereas the *High* hydrogel variant displayed a significantly reduced D_w (99.48±15.11 $\mu m^2/s$) (**Fig. 2C**). Hydrogel mesh sizes (ξ) inversely mirrored that of the moduli, with decreased mesh size associated with increased GelMA content: ξ_{low}=72, ξ_{med}=58, ξ_{high}=32nm (**Fig. 2D**).

3.2. MSC mediated remodeling of GelMA hydrogels

We subsequently quantified MSC remodeling of the *Low*, *Med*, and *High* hydrogels via compressive tests as a function of time in culture (0 – 7 days) and MSC seeding density (0, $1x10^5$, $1x10^6$ cells/mL), with results reported as absolute values as well as normalized against the initial properties (day 0) of each variant (**Fig. 3B**). Notably, no observable trends in modulus change were observed over time at either MSC seeding density for *Low* and *Med* hydrogels variants. However, the *High* hydrogel (7.5%GelMA; 85% DOF; 0.1%PI) displayed significant remodeling over time for the highest MSC seeding density ($1x10^6$ MSCs/mL). Here, significant biosynthetic remodeling was observed, characterized by significant increases in Young's

modulus (ΔE = 2.61±0.72), almost twice that of other seeding conditions (ΔE = 1.13±0.45, acellular; ΔE = 1.25±0.13, $1x10^5$ MSCs/mL). For all other hydrogel and seeding conditions, the bulk Young's modulus did not change significantly over time (**Fig. 3A**).

We then examined expression of a panel of remodeling associated gene, with results displayed on a log_2 color scale where upregulated genes are shown in blue, downregulated genes in red, and non-determinant values in gray. Remodeling associated genes were largely downregulated in MSCs as early as day 1, however there were a number of interesting trends across groups. The MMP-activity repressor, tissue inhibitor of metalloprotease TIMP-1 showed modest upregulation as a function of MSC seeding density at day 1 (1.3-fold for 1:1 MSC cultures, $1x10^5$

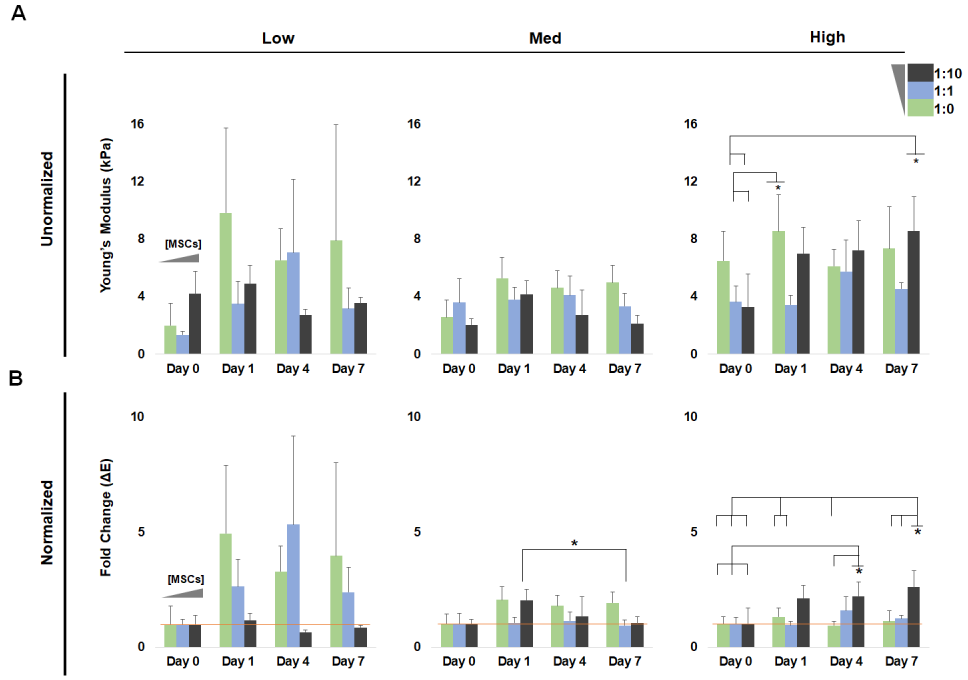

Figure 3. Bulk Young's modulus of *Low*, *Med*, and *High* hydrogels cultured over 7 days with seeding densities of 0, $1x10^5$, and $1x10^6$ MSCs/mL (1:0, 1:1, 1:10 HSCPs:MSCs). (**n=3-6**). **A)** There is minimal change in Young's modulus over time in any hydrogel and seeding conditions. The high hydrogel shows a significant increase ($p<0.05$) from initial seeding to day 7 in the presence of a high concentration of the highest density of MSCs, $1x10^6$ MSCs/mL. **B)** The Young's modulus was normalized to the initial value, day 0, of the specific seeding and hydrogel variant to show fold change. This highlights that only the *High* with the highest concentration of MSCs ($1x10^6$ MSCs/mL) experiences significant increase ($p<0.05$) in bulk Young's modulus over time.

MSCs/mL; 1.5-fold for 1:10 MSC cultures, $1x10^6$ MSCs/mL) for each hydrogel condition (*Low*, *Med*, *High*), however this fell off by day 4 and TIMP-1 became downregulated. MMP-9 saw the largest upregulation with around 6-fold increase on day 1 across all hydrogel variants in the lowest seeding density (**Fig. 4A**). The high seeding density, $1x10^6$ MSCs/mL had higher MMP-9 upregulation, with 10.8±1.93 fold increase on day 1 in the *Low* hydrogel (**Fig. 4B**). TIMP-3 was sharply downregulated, dropping to near zero-fold expression by day 1. TIMP-2 and Col1(α1) also fell to near zero by day 4, withTIMP-2 having sufficiently low yields on day 1 to be

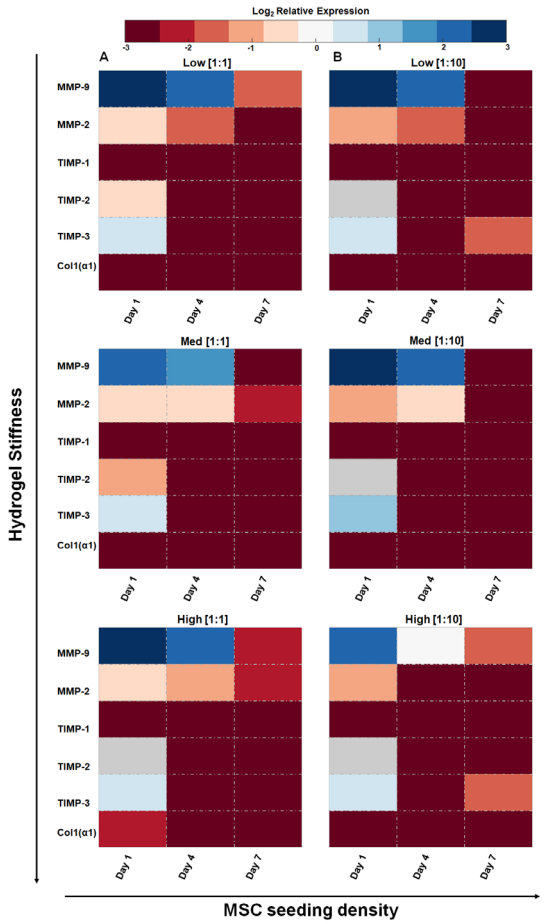

Figure 4. Relative gene expression of matrix-associated genes normalized to day 0 expression, shown on a log2 scale, with downregulation shown in red and upregulation shown in blue. Gray values for TIMP-2 show non-determinant values, indicative of low yields of expression. Matrix degradation genes analyzed were matrix metalloproteases MMP-2 and MMP-9. Matrix additive genes were the tissue inhibitors of metalloproteases TIMP-1, TIMP-2, and TIMP-3, along with the matrix protein collagen, type 1, alpha 1. (**n=3-6**). **A)** Gene expression of hydrogels seeded with low density of MSCs $1x10^5$ MSCs/mL (1:1 HSCPs:MSC). **B)** Gene expression of hydrogels seeded with high density of MSCs $1x10^6$ MSCs/mL (1:10 HSCPs:MSCs).

undetermined by PCR. MMP-2 decreased as well, reducing by a 0.7-fold change ($1x10^5$ MSCs/mL) (**Fig. 4A)** and 0.4-fold change ($1x10^6$ MSCs/mL) (**Fig. 4B)** by day 1.

3.3 Culture system dependent hematopoietic differentiation patterns

Analysis of the HSPC–only hydrogel culture shows an HSC population dependence on hydrogel condition: *Low*, *Med*, and *High* (**Fig. 5B,C)**. The percentage of HSCs followed an inverse trend with increasing GelMA concentration, falling from 2.85±0.67%, to 1.10±0.70%, to 0.21±0.19% in the *Low*, *Med*, and *High* hydrogels respectively (**Fig. 5C)**. Not unexpectedly, there was an associated increase in the downstream cell population patterns with the decrease in early progenitors. This was seen in the Common Myeloid Progenitors (CMP) cell population which made up 4.95±1.02% of the hematopoietic cell population in the *Low* hydrogel, but was significantly larger in the *High* hydrogel, 13.72±2.93% (**Fig. 5B)**. A similar trend was seen in the Terminal cell population, in which increasing GelMA content led to increasing hematopoietic

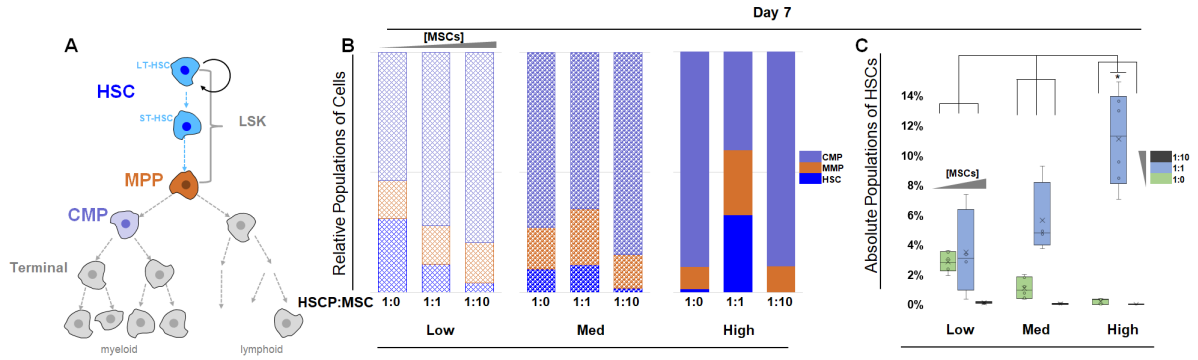

Figure 5. Analysis of cell populations at day 7 (**n=6**). **A)** The lineage hierarchy of hematopoietic stem cells, with long-term and short-term hematopoietic stem cells grouped as HSCs (blue), Multipotent Progenitors (orange), and Common Myeloid Progenitors (lavender). **B)** The relative population of HSC (blue), MPP (orange), CMP (lavender) are shown for single-culture and co-culture at 1:1 and 1:10 (HSCPs:MSCs), in the *Low, Med,* and *High* variants. The height of each subcolumn reflects how much of the total cell population is made up of the specified cell type. The blue columns (HSC) show that the highest percentage of HSCs are found in the single-culture *Low* variant (1:0), and in the 1:1 co-culture *High* variant. **C)** The percentage of HSCs that make up the total hematopoietic cell population, arranged in order of increasing MSC density (1:0, 1:1, 1:10 HSCPs:MSC), and in order of increasing hydrogel stiffness (*Low*, *Med*, and *High*). The largest percent of HSC is found in the *High* variant l at a 1:1 seeding ratio, and is significantly higher (p=0.05) than all other conditions.

terminal cell population (**Fig. S6)**.

When HSPCs were co-cultured with MSCs there were important shifts in HSC differentiation patterns (**Fig. 5)**. Where previously the highest final percentage of early progenitor cells was found in the low GelMA hydrogels, the addition of MSCs in a 1:1 [HSCPs:MSCs] ratio created a reversal in that trend. The highest maintenance was found in the *High* hydrogel variant with HSCs comprising 11.11±3.18% of the hematopoietic population, while the fraction of remaining

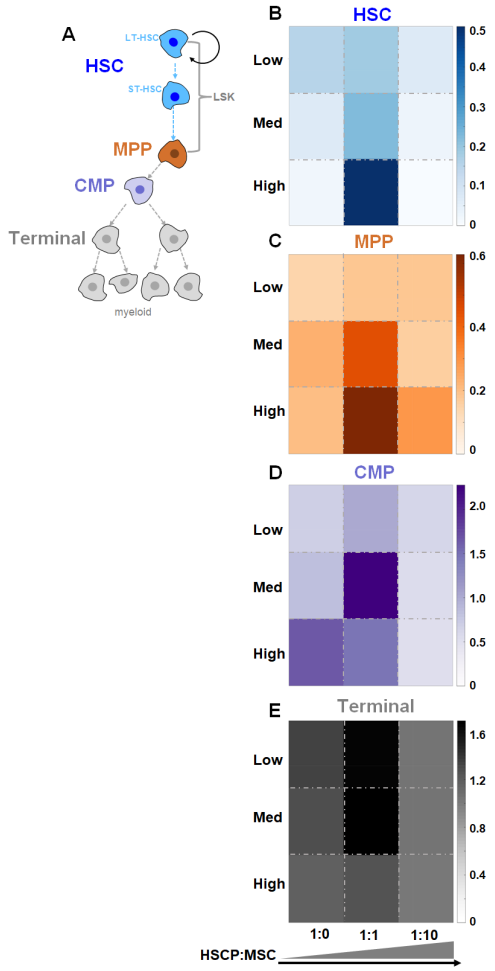

Figure 6. Relative fold change of cell population from day 1 to day 7 **A)** Color-coded hematopoietic lineage hierarchy **B)** Fold change of HSC population. Darker blue indicates higher maintenance of HSC (highest maintenance in *High* variant at 1:1 seeding). **C)** Fold change of MPP population. Darker orange indicates higher maintenance of MPP (highest in *High* variant at 1:1 seeding). **D)** Fold change of CMP population. Darker purple indicates higher maintenance of CMP (highest in *Med* variant at 1:1 seeding). **E)** Fold change of Terminal population. Darker gray indicates higher maintenance of Terminal population (highest in *Med* variant at 1:1 seeding).

HSCs was significantly lower in the *Med* and *Low* variants (**Fig. 5B,C)**. From day 1 to day 7 this represents maintenance of 50.2%, 22.08%, and 18.50% of the initial HSC population for *High*, *Med*, and *Low* (**Fig. 6)**. Comparatively, higher HSC maintenance led to a lower Terminal cell population of 77.54±5.83% for *High* hydrogel variants (compared to 82.70±6.09% and 91.50±4.67% for *Med* and *Low* hydrogel variants; **Fig. S6)**. When HSCPs were co-cultured with a higher density of MSCs ($1x10^6$ MSCs/mL), at a ratio of 1:10 [HSCPs:MSC], hematopoietic differentiation towards late-stage lineage was enhanced (**Fig. 5B,C)**. Not surprisingly, terminal cells made up the bulk of the hematopoietic population, representing more than 99% of the hematopoietic cells (**Fig. S6)**.

4. Discussion

Synthetic niche analogs for *ex vivo* culture of HSCs have begun to uncouple the complex signals inherent to the native HSC *in vivo* niche. More traditional efforts have demonstrated that changes in matrix composition, mechanics, and selective inclusion of growth factors can substantially alter HSC maintenance and differentiation patterns. Notably, selective interactions with fibronectin [84-86], or immobilization of SCF within a hydrogel [46, 87, 88], can enhance HSC maintenance. More recently, the concept of cell-cell signaling and its role on HSC lineage specification have begun to be examined, primarily in diffusion-unlimited experimental systems. Notably, *Csaszar et al.* demonstrated that HSC-secreted cytokines can alter *ex vivo* expansion of HSCs in liquid culture within a bioreactor [27], while *Müller et al.* demonstrated that autocrine feedback associated with HSCs cultured individually in microcavities led to increased HSC quiescence [89]. However, it is also important to consider the influence of heterotypic cell-cell interactions within more complex niche mimics. In this situation, 3D hydrogel biomaterials are particularly advantageous as heterotypic cell-cell cultures can be maintained in an environment where the kinetics of HSC-generated autocrine feedback versus paracrine signaling from niche-associated cells can be manipulated by the poroelastic properties of the hydrogel itself.

Recently, we described the use of a collagen hydrogel system to examine feedback between HSCs and Lin^+ niche cells isolated from the bone marrow in regards to HSC proliferation and myeloid lineage specification. Notably, while paracrine signals from Lin^+ cells induce HSC myeloid differentiation in high-diffusivity environments, diffusion-limited hydrogel environments promoted autocrine feedback and HSC maintenance [29].

However, the hydrogel matrix that facilitates studies of the influence of autocrine feedback vs. heterotypic paracrine signals on HSC activity may also be sensitive to cell-mediated remodeling. In this regard, concepts of dynamic reciprocity, often employed in the context of wound remodeling or the tumor microenvironment [90, 91], offer a novel avenue to explore the design of HSC culture platforms. Therefore, we developed a culture system that takes advantage of paracrine signaling from niche-associated mesenchymal stromal cells (MSCs). Our application of a library of GelMA hydrogels that span the range of elastic moduli found within the native HSC niche [17], as well as advanced poroelastic characterization methods [50, 52], allows us to examine dynamic relationships between MSCs, the local matrix architecture, and autocrine versus paracrine domains. HSCPs were co-cultured with MSCs at varying ratios (1:0, 1:1, 1:10 HSCPs:MSCs) to demonstrate that HSC differentiation patterns can be manipulated by combinations of initial hydrogel properties, MSC mediated remodeling, and the balance of autocrine feedback versus MSC-generated paracrine signals.

Gelatin was chosen as the base material of our system given its inherent ability for cell interaction. It possesses cleavage sites for matrix metalloproteinases produced by MSCs and RGD adhesion sites [45]. Methacrylamide-functionalization and subsequent crosslinking of GelMA eliminates the problem of gelatin instability at elevated temperatures. The mechanical properties of the GelMA hydrogels encompassed the range of moduli observed in the native bone marrow niche (**Fig. 2**). In terms of biotransport the *Low* and *Med* versus *High* hydrogels

displayed two subsets of diffusion and mesh size. Notably, based on previous result from *Mahadik et al*. [29] the poor diffusivity of the *High* hydrogel suggests an autocrine-dominated regime for HSC culture characterized by a small radius of cell-secreted chemical diffusion [92]. Similarly, the significantly increased diffusivity of the *Low* and *Med* hydrogels suggests a regime for HSC culture characterized by a large radius of cell-secreted chemical diffusion to reduce the effects of autocrine feedback and enhance MSC-generated paracrine signaling.

We observed HSC maintenance was strongly influenced by initial hydrogel poroelastic properties, the presence of MSCs, and MSC-associated remodeling processes. When cultured on their own, HSC maintenance was greatest in high diffusion, low stiffness hydrogels (*Low*) (**Fig. 5**). To explore the influence of paracrine signals from niche-associated MSCs, we subsequently examined HSC lineage specification patterns in the same set of *Low*, *Med*, and *High* hydrogels as a result of co-culture with MSCs at either $1x10^5$ or $1x10^6$ MSCs/mL (1:1, 1:10 HSCPs:MSCs). The addition of cells did not significantly alter the initial Young's modulus (**Fig. 3)**. The presence of MSCs yielded significant, dynamic matrix remodeling as seen via downregulated matrix deposition related genes (Col1(α1), TIMP-1, TIMP-2, TIMP-3) and upregulated matrix degradation genes (MMP-2, MMP-9) (**Fig. 4**). Together, these results suggest substantial changes in mesh size and biotransport. While we observed significant matrix remodeling via repeated compressive testing in *High* hydrogels seeded with the highest MSC density, no clear trends were observed in the *Low* or *Med* conditions. Recent results from *Schultz et al.* described non-uniform matrix remodeling [93] as a result of differences in diffusive path lengths and reaction times for MMPs vs. TIMPs. This suggests remodeling of our hydrogels was likely non-uniform, making it difficult to resolve local remodeling processes within the heterotypic HSC-MSC cultures. However, the significant changes in HSC activity observed as a result of co-culture of MSCs suggest dynamic interaction between HSCs and MSCs is an exciting avenue for further exploration.

Addition of large populations of MSCs (1:10 HSCPs:MSCs) led to a decrease in HSC maintenance for all hydrogel variants. This suggests oversaturation by MSCs likely leads to not only increased paracrine signals but also significantly greater remodeling, resulting in a loss in the ability to maintain early hematopoietic progenitors as compared to HSC-only cultures (**Fig. 5)**. However, addition of an equivalent amount of MSCs (1:1 HSCPs:MSCs) leads to a very different shift in HSC population dynamics, with an overwhelming increase in HSC maintenance. This increase aligns with literature, indicating the ability of MSCs to influence HSC equilibrium through secreted factors and direct cell-cell contact [31]. Notably, highest maintenance of HSCs in the 1:1 HSCPs:MSCs culture was observed in the *High* hydrogel variant that displayed minimal initial biotransport capabilities but also long-term signatures of MSC-mediated remodeling (MMP-9 expression). This suggests the importance of a balance between initial autocrine-dominated feedback followed by MSC paracrine signals for increasing HSC maintenance. These findings highlight the possibility for selectively employing more complex culture systems to engineer HSC lineage specification patterns.

Taken together, this work shows that for the maintenance of the HSC population, the presence of niche-associated MSCs is desirable, but oversaturation of MSC-HSC signaling can lead to significant early progenitor loss. Through tuning biomaterial parameters, a diffusion-limited GelMA matrix with 1x MSCs was found to maintain a higher percent of early hematopoietic progenitor cells. Remodeling of the matrix by MSCs occurs locally, and can increase the possibility of paracrine interactions with HSCs over time. Overall, this suggests that for maintenance of the HSC population *ex vivo* MSC-HSC interactions play a pivotal role in concentration dependent signaling pathways with dynamic shifts in autocrine and paracrine signaling.

5. Conclusions

Bone marrow niches contain a complex milieu of external signals that play a significant role in to mediating the activity of HSCs *in vivo*. The development of a synthetic niche analog for HSC culture can take advantage of poroelastic properties to mediate the balance of autocrine and paracrine signaling mechanisms. Here, we explored the use of MSC-secreted paracrine signaling as well as MSC-mediated matrix remodeling as a means to increase HSC maintenance during in vitro culture using a library of GelMA hydrogels. Examining HSC differentiation patterns as well as dynamic remodeling of a model GelMA hydrogel in the presence of MSCs suggests a path towards *ex vivo* expansion of HSCs. We show that combinations of initial hydrogel properties and a moderate amount of MSCs increases the maintenance of HSCs in a culture system with initially hindered diffusion. These findings suggest that MSC-secreted paracrine signaling and initial autocrine feedback are essential for *in vitro* tools seeking to expand HSC populations. Such findings offer exciting opportunities to explore concepts of dynamic reciprocity in the context of heterotypic cell cultures. Matrix remodeling as well as selective domains of autocrine feedback versus paracrine signaling can be leveraged for the intelligent design of an *in vitro* HSC culture systems.

Acknowledgements

The authors would like to acknowledge Dr. Barbara Pilas of the Roy J. Carver Biotechnology Center (Flow Cytometry Facility, UIUC) as well as Dr. Bhushan Mahadik and Dr. Ji-Sun Choi (ChBE, UIUC) for assistance with bone marrow cell isolation and flow cytometry. Preliminary Young's modulus testing and mRNA extraction was aided by undergraduate researchers Kirsten Schroeder and Gabrielle Wolter respectively. Research reported in this publication was supported by the National Institute of Diabetes and Digestive and Kidney Diseases of the National Institutes of Health under Award Number R01 DK099528 (B.A.C.H) and R21 EB018481 (B.A.C.H.). Amino Acid Analysis was performed at the Molecular Structure Facility in the UC Davis Genome Center at the University of California, Davis. Material characterization

was carried out in part in the Frederick Seitz Materials Research Laboratory Central Research Facilities, University of Illinois. The authors are also grateful for additional funding provided by the Department of Chemical & Biomolecular Engineering and the Institute for Genomic Biology at the University of Illinois at Urbana-Champaign.

Data Availability

All data analyzed during this study are included in this published article (and its supplementary information files). Raw data required to reproduce these findings are available from the corresponding author on reasonable request.

Declarations of Interest

Declarations of interest: none

References

[1] J. Holst, S. Watson, M.S. Lord, S.S. Eamegdool, D.V. Bax, L.B. Nivison-Smith, A. Kondyurin, L. Ma, A.F. Oberhauser, A.S. Weiss, J.E. Rasko, Substrate elasticity provides mechanical signals for the expansion of hemopoietic stem and progenitor cells, Nat Biotechnol 28(10) (2010) 1123-8.
[2] C. Lee-Thedieck, N. Rauch, R. Fiammengo, G. Klein, J.P. Spatz, Impact of substrate elasticity on human hematopoietic stem and progenitor cell adhesion and motility, J Cell Sci 125(Pt 16) (2012) 3765-75.
[3] M. Krater, A. Jacobi, O. Otto, S. Tietze, K. Muller, D.M. Poitz, S. Palm, V.M. Zinna, U. Biehain, M. Wobus, T. Chavakis, C. Werner, J. Guck, M. Bornhauser, Bone marrow niche-mimetics modulate HSPC function via integrin signaling, Sci Rep 7(1) (2017) 2549.
[4] J.A. LaIuppa, T.A. McAdams, E.T. Papoutsakis, W.M. Miller, Culture materials affectex vivo expansion of hematopoietic progenitor cells, Journal of Biomedical Materials Research 36(3) (1997) 347-359.
[5] E.M. Pietras, M.R. Warr, E. Passegue, Cell cycle regulation in hematopoietic stem cells, J Cell Biol 195(5) (2011) 709-20.
[6] A. Wilson, A. Trumpp, Bone-marrow haematopoietic-stem-cell niches, Nat Rev Immunol 6(2) (2006) 93-106.
[7] S.J. Morrison, D.T. Scadden, The bone marrow niche for haematopoietic stem cells, Nature 505(7483) (2014) 327-34.
[8] G.B. Adams, D.T. Scadden, The hematopoietic stem cell in its place, Nat Immunol 7(4) (2006) 333-7.
[9] L.E. Purton, D.T. Scadden, The hematopoietic stem cell niche, StemBook, Cambridge (MA), 2008.
[10] D.S. Krause, D.T. Scadden, F.I. Preffer, The hematopoietic stem cell niche--home for friend and foe?, Cytometry B Clin Cytom 84(1) (2013) 7-20.
[11] E.A. Copelan, Hematopoietic stem-cell transplantation, N Engl J Med 354(17) (2006) 1813-26.
[12] A. D'Souza, X. Zhu, Current Uses and Outcomes of Hematopoietic Cell Transplantation (HCT): CIBMTR Summary Slides, 2016.
[13] J. Zhang, L. Li, Stem cell niche: microenvironment and beyond, J Biol Chem 283(15) (2008) 9499-503.
[14] (!!! INVALID CITATION !!! [4-9]).
[15] C. Nombela-Arrieta, G. Pivarnik, B. Winkel, K.J. Canty, B. Harley, J.E. Mahoney, S.-Y. Park, J. Lu, A. Protopopov, L.E. Silberstein, Quantitative imaging of haematopoietic stem and progenitor cell localization and hypoxic status in the bone marrow microenvironment, Nat Cell Biol 15(5) (2013) 533-543.
[16] S.K. Nilsson, M.E. Debatis, M.S. Dooner, J.A. Madri, P.J. Quesenberry, P.S. Becker, Immunofluorescence characterization of key extracellular matrix proteins in murine bone marrow in situ, J Histochem Cytochem 46(3) (1998) 371-7.
[17] L.E. Jansen, N.P. Birch, J.D. Schiffman, A.J. Crosby, S.R. Peyton, Mechanics of intact bone marrow, J Mech Behav Biomed Mater 50 (2015) 299-307.
[18] J.A. LaIuppa, T.A. McAdams, E.T. Papoutsakis, W.M. Miller, Culture materials affect ex vivo expansion of hematopoietic progenitor cells, Journal of Biomedical Materials Research 36(3) (1997) 347-359.
[19] J.S. Choi, B.A. Harley, Marrow-inspired matrix cues rapidly affect early fate decisions of hematopoietic stem and progenitor cells, Sci Adv 3(1) (2017) e1600455.
[20] A. Janowska-Wieczorek, M. Majka, J. Ratajczak, M.Z. Ratajczak, Autocrine/paracrine mechanisms in human hematopoiesis, Stem Cells 19(2) (2001) 99-107.
[21] M. Majka, A. Janowska-Wieczorek, J. Ratajczak, K. Ehrenman, Z. Pietrzkowski, M.A.

Kowalska, A.M. Gewirtz, S.G. Emerson, M.Z. Ratajczak, Numerous growth factors, cytokines, and chemokines are secreted by human CD34(+) cells, myeloblasts, erythroblasts, and megakaryoblasts and regulate normal hematopoiesis in an autocrine/paracrine manner, Blood 97(10) (2001) 3075-85.
[22] T. Stylianopoulos, M.Z. Poh, N. Insin, M.G. Bawendi, D. Fukumura, L.L. Munn, R.K. Jain, Diffusion of particles in the extracellular matrix: the effect of repulsive electrostatic interactions, Biophys J 99(5) (2010) 1342-9.
[23] P. Kamali-Zare, C. Nicholson, Brain extracellular space: geometry, matrix and physiological importance, Basic Clin Neurosci 4(4) (2013) 282-6.
[24] A. Pluen, P.A. Netti, R.K. Jain, D.A. Berk, Diffusion of Macromolecules in Agarose Gels: Comparison of Linear and Globular Configurations, Biophysical Journal 77(1) (1999) 542-552.
[25] C.C. van Donkelaar, G. Chao, D.L. Bader, C.W. Oomens, A reaction-diffusion model to predict the influence of neo-matrix on the subsequent development of tissue-engineered cartilage, Comput Methods Biomech Biomed Engin 14(5) (2011) 425-32.
[26] S. Taqvi, L. Dixit, K. Roy, Biomaterial-based notch signaling for the differentiation of hematopoietic stem cells into T cells, J Biomed Mater Res A 79(3) (2006) 689-97.
[27] E. Csaszar, Daniel C. Kirouac, M. Yu, W. Wang, W. Qiao, Michael P. Cooke, Anthony E. Boitano, C. Ito, Peter W. Zandstra, Rapid expansion of human hematopoietic stem cells by automated control of inhibitory feedback signaling, Cell Stem Cell 10(2) (2012) 218-229.
[28] E. Muller, W. Wang, W. Qiao, M. Bornhauser, P.W. Zandstra, C. Werner, T. Pompe, Distinguishing autocrine and paracrine signals in hematopoietic stem cell culture using a biofunctional microcavity platform, Sci Rep 6 (2016) 31951.
[29] B.P. Mahadik, N.A. Bharadwaj, R.H. Ewoldt, B.A. Harley, Regulating dynamic signaling between hematopoietic stem cells and niche cells via a hydrogel matrix, Biomaterials 125 (2017) 54-64.
[30] A. Ehninger, A. Trumpp, The bone marrow stem cell niche grows up: mesenchymal stem cells and macrophages move in, J Exp Med 208(3) (2011) 421-8.
[31] S. Mendez-Ferrer, T.V. Michurina, F. Ferraro, A.R. Mazloom, B.D. Macarthur, S.A. Lira, D.T. Scadden, A. Ma'ayan, G.N. Enikolopov, P.S. Frenette, Mesenchymal and haematopoietic stem cells form a unique bone marrow niche, Nature 466(7308) (2010) 829-34.
[32] T. Sugiyama, H. Kohara, M. Noda, T. Nagasawa, Maintenance of the hematopoietic stem cell pool by CXCL12-CXCR4 chemokine signaling in bone marrow stromal cell niches, Immunity 25(6) (2006) 977-88.
[33] M. Ogawa, Differentiation and proliferation of hematopoietic stem cells, Blood 81(11) (1993) 2844-53.
[34] C. Mirantes, E. Passegue, E.M. Pietras, Pro-inflammatory cytokines: emerging players regulating HSC function in normal and diseased hematopoiesis, Exp Cell Res 329(2) (2014) 248-54.
[35] A. Tocci, L. Forte, Mesenchymal stem cell: use and perspectives, Hematol J 4(2) (2003) 92-6.
[36] B.A. Anthony, D.C. Link, Regulation of hematopoietic stem cells by bone marrow stromal cells, Trends Immunol 35(1) (2014) 32-7.
[37] T. Li, Y. Wu, Paracrine molecules of mesenchymal stem cells for hematopoietic stem cell niche, Bone Marrow Res 2011 (2011) 353878.
[38] W. Wagner, C. Roderburg, F. Wein, A. Diehlmann, M. Frankhauser, R. Schubert, V. Eckstein, A.D. Ho, Molecular and secretory profiles of human mesenchymal stromal cells and their abilities to maintain primitive hematopoietic progenitors, Stem Cells 25(10) (2007) 2638-47.
[39] S. El Marsafy, Mesenchymal Stem Cells: Pivotal Players in Hematopoietic Stem Cell Microenvironment, Journal of Stem Cell Research & Therapy 04(08) (2014).
[40] W.P. Daley, S.B. Peters, M. Larsen, Extracellular matrix dynamics in development and regenerative medicine, J Cell Sci 121(Pt 3) (2008) 255-64.

[41] G.S. Schultz, J.M. Davidson, R.S. Kirsner, P. Bornstein, I.M. Herman, Dynamic reciprocity in the wound microenvironment, Wound Repair Regen 19(2) (2011) 134-48.
[42] A. Page-McCaw, A.J. Ewald, Z. Werb, Matrix metalloproteinases and the regulation of tissue remodelling, Nat Rev Mol Cell Biol 8(3) (2007) 221-33.
[43] C. Sassoli, D. Nosi, A. Tani, F. Chellini, B. Mazzanti, F. Quercioli, S. Zecchi-Orlandini, L. Formigli, Defining the role of mesenchymal stromal cells on the regulation of matrix metalloproteinases in skeletal muscle cells, Exp Cell Res 323(2) (2014) 297-313.
[44] J.A. Benton, C.A. DeForest, V. Vivekanandan, K.S. Anseth, Photocrosslinking of gelatin macromers to synthesize porous hydrogels that promote valvular interstitial cell function, Tissue Eng Part A 15(11) (2009) 3221-30.
[45] S. Pedron, B.A. Harley, Impact of the biophysical features of a 3D gelatin microenvironment on glioblastoma malignancy, J Biomed Mater Res A 101(12) (2013) 3404-15.
[46] B.P. Mahadik, S. Pedron Haba, L.J. Skertich, B.A. Harley, The use of covalently immobilized stem cell factor to selectively affect hematopoietic stem cell activity within a gelatin hydrogel, Biomaterials 67 (2015) 297-307.
[47] J.E. Chen, S. Pedron, B.A.C. Harley, The Combined Influence of Hydrogel Stiffness and Matrix-Bound Hyaluronic Acid Content on Glioblastoma Invasion, Macromol Biosci 17(8) (2017).
[48] A. International, ASTM E111-17 Standard Test Method for Young's Modulus, Tangent Modulus, and Chord Modulus, ASTM International, 2017.
[49] S. Pedron, E. Becka, B.A. Harley, Regulation of glioma cell phenotype in 3D matrices by hyaluronic acid, Biomaterials 34(30) (2013) 7408-17.
[50] Z.I. Kalcioglu, R. Mahmoodian, Y. Hu, Z. Suo, K.J. Van Vliet, From macro- to microscale poroelastic characterization of polymeric hydrogels via indentation, Soft Matter 8(12) (2012).
[51] Y.H. Hu, X. Chen, G.M. Whitesides, J.J. Vlassak, Z.G. Suo, Indentation of polydimethylsiloxane submerged in organic solvents, Journal of Materials Research 26(6) (2011) 785-795.
[52] Y. Hu, X. Zhao, J.J. Vlassak, Z. Suo, Using indentation to characterize the poroelasticity of gels, Applied Physics Letters 96(12) (2010).
[53] Y. Lai, Y. Hu, Unified solution for poroelastic oscillation indentation on gels for spherical, conical and cylindrical indenters, Soft Matter 13(4) (2017) 852-861.
[54] N.A. Peppas, E.W. Merrill, Crosslinked poly(vinyl alcohol) hydrogels as swollen elastic networks, Journal of Applied Polymer Science 21(7) (1977) 1763-1770.
[55] J.C. Bray, E.W. Merrill, Poly(vinyl alcohol) hydrogels. Formation by electron beam irradiation of aqueous solutions and subsequent crystallization, Journal of Applied Polymer Science 17(12) (1973) 3779-3794.
[56] T. Canal, N.A. Peppas, Correlation between mesh size and equilibrium degree of swelling of polymeric networks, J Biomed Mater Res 23(10) (1989) 1183-93.
[57] J.E. Schiel, D.S. Hage, Density measurements of potassium phosphate buffer from 4 to 45 degrees C, Talanta 65(2) (2005) 495-500.
[58] I.G. Fels, Hydration and density of collagen and gelatin, Journal of Applied Polymer Science 8(4) (1964) 1813-1824.
[59] J.H. Fessler, A.J. Hodge, Ultracentrifugal observation of phase transitions in density gradients, Journal of Molecular Biology 5(4) (1962) 446-IN2.
[60] F. Anjum, P.S. Lienemann, S. Metzger, J. Biernaskie, M.S. Kallos, M. Ehrbar, Enzyme responsive GAG-based natural-synthetic hybrid hydrogel for tunable growth factor delivery and stem cell differentiation, Biomaterials 87 (2016) 104-17.
[61] P.J. Flory, J. Rehner, Statistical Mechanics of Cross-Linked Polymer Networks II. Swelling, The Journal of Chemical Physics 11(11) (1943) 521-526.
[62] W. Burchard, Light Scattering Techniques, Physical Techniques for the Study of Food Biopolymers1994, pp. 151-213.
[63] J.D. Bryngelson, E.M. Billings, From interatomic interactions to protein structure, Physics of

Biological Systems, Springer1997, pp. 80-116.
[64] G.A. Challen, N. Boles, K.K.Y. Lin, M.A. Goodell, Mouse Hematopoietic Stem Cell Identification and Analysis, Cytom Part A 75a(1) (2009) 14-24.
[65] L. Yang, D. Bryder, J. Adolfsson, J. Nygren, R. Mansson, M. Sigvardsson, S.E. Jacobsen, Identification of Lin(-)Sca1(+)kit(+)CD34(+)Flt3- short-term hematopoietic stem cells capable of rapidly reconstituting and rescuing myeloablated transplant recipients, Blood 105(7) (2005) 2717-23.
[66] S. Okada, H. Nakauchi, K. Nagayoshi, S.I. Nishikawa, Y. Miura, T. Suda, Invivo and Invitro Stem-Cell Function of C-Kit-Positive and Sca-1-Positive Murine Hematopoietic-Cells, Blood 80(12) (1992) 3044-3050.
[67] J.S. Choi, B.P. Mahadik, B.A. Harley, Engineering the hematopoietic stem cell niche: Frontiers in biomaterial science, Biotechnol J 10(10) (2015) 1529-45.
[68] B.P. Mahadik, T.D. Wheeler, L.J. Skertich, P.J.A. Kenis, B.A.C. Harley, Microfluidic Generation of Gradient Hydrogels to Modulate Hematopoietic Stem Cell Culture Environment, Advanced Healthcare Materials 3(3) (2014) 449-458.
[69] A.E. Beaudin, S.W. Boyer, E.C. Forsberg, Flk2/Flt3 promotes both myeloid and lymphoid development by expanding non-self-renewing multipotent hematopoietic progenitor cells, Exp Hematol 42(3) (2014) 218-229 e4.
[70] Y. Ilin, J.S. Choi, B.A. Harley, M.L. Kraft, Identifying States along the Hematopoietic Stem Cell Differentiation Hierarchy with Single Cell Specificity via Raman Spectroscopy, Anal Chem 87(22) (2015) 11317-24.
[71] L.P. Yang, D. Bryder, J. Adolfsson, J. Nygren, R. Mansson, M. Sigvardsson, S.E.W. Jacobsen, Identification of Lin(-)Sca1(+)kit(+)CD34(+)Flt(3-) short-term hematopoietic stem cells capable of rapidly reconstituting and rescuing myeloablated transplant recipients, Blood 105(7) (2005) 2717-2723.
[72] C. Tian, Y. Zhang, Purification of hematopoietic stem cells from bone marrow, Ann Hematol 95(4) (2016) 543-7.
[73] Y. Zhang, X. Yan, G. Sashida, X. Zhao, Y. Rao, S. Goyama, S.P. Whitman, N. Zorko, K. Bernot, R.M. Conway, D. Witte, Q.F. Wang, D.G. Tenen, Z. Xiao, G. Marcucci, J.C. Mulloy, H.L. Grimes, M.A. Caligiuri, G. Huang, Stress hematopoiesis reveals abnormal control of self-renewal, lineage bias, and myeloid differentiation in Mll partial tandem duplication (Mll-PTD) hematopoietic stem/progenitor cells, Blood 120(5) (2012) 1118-29.
[74] G.A. Challen, N. Boles, K.K. Lin, M.A. Goodell, Mouse hematopoietic stem cell identification and analysis, Cytometry A 75(1) (2009) 14-24.
[75] A. Mayle, M. Luo, M. Jeong, M.A. Goodell, Flow cytometry analysis of murine hematopoietic stem cells, Cytometry A 83(1) (2013) 27-37.
[76] G.J. Spangrude, S. Heimfeld, I.L. Weissman, Purification and characterization of mouse hematopoietic stem cells, Science 241(4861) (1988) 58-62.
[77] Guide to performing relative quantification of gene expression using real-time quantitative PCR, Part Number 4371095, Rev. B, Applied Biosystems, www.docs.appliedbiosystems.com, 2008.
[78] L.C. Abraham, J.F. Dice, K. Lee, D.L. Kaplan, Phagocytosis and remodeling of collagen matrices, Exp Cell Res 313(5) (2007) 1045-55.
[79] A. Ghasemi, S. Zahediasl, Normality tests for statistical analysis: a guide for non-statisticians, Int J Endocrinol Metab 10(2) (2012) 486-9.
[80] R.J. Carroll, H. Schneider, A note on levene's tests for equality of variances, Statistics & Probability Letters 3(4) (1985) 191-194.
[81] J. Cohen, Statistical power analysis for the behavioral sciences, 2nd ed. ed., L. Erlbaum Associates, Hillsdale, N.J. :, 1988.
[82] J. Cohen, A power primer, Psychol Bull 112(1) (1992) 155-9.
[83] R.B. Dean, W.J. Dixon, Simplified Statistics for Small Numbers of Observations, Analytical

Chemistry 23(4) (1951) 636-638.
[84] J.S. Choi, B.A.C. Harley, Marrow-inspired matrix cues rapidly affect early fate decisions of hematopoietic stem and progenitor cells, Science Advances 3(1) (2017) e1600455.
[85] J.S. Choi, B.A.C. Harley, Substrate elasticity and chmistry regulate the biophysical properties and lineage commitment of hematopoietic stem cells, In preparation (2013).
[86] E. Altrock, C.A. Muth, G. Klein, J.P. Spatz, C. Lee-Thedieck, The significance of integrin ligand nanopatterning on lipid raft clustering in hematopoietic stem cells, Biomaterials 33(11) (2012) 3107-18.
[87] M.L. Cuchiara, S. Coşkun, O.A. Banda, K.L. Horter, K.K. Hirschi, J.L. West, Bioactive poly(ethylene glycol) hydrogels to recapitulate the HSC niche and facilitate HSC expansion in culture, Biotechnol Bioeng 113(4) (2016) 870-881.
[88] M.L. Cuchiara, K.L. Horter, O.A. Banda, J.L. West, Covalent immobilization of stem cell factor and stromal derived factor 1alpha for in vitro culture of hematopoietic progenitor cells, Acta Biomater 9(12) (2013) 9258-69.
[89] E. Müller, W. Wang, W. Qiao, M. Bornhäuser, P.W. Zandstra, C. Werner, T. Pompe, Distinguishing autocrine and paracrine signals in hematopoietic stem cell culture using a biofunctional microcavity platform, Sci Rep 6 (2016) 31951.
[90] J. Alexander, E. Cukierman, Stromal dynamic reciprocity in cancer: intricacies of fibroblastic-ECM interactions, Current Opinion in Cell Biology 42 (2016) 80-93.
[91] G.S. Schultz, J.M. Davidson, R.S. Kirsner, P. Bornstein, I.M. Herman, Dynamic reciprocity in the wound microenvironment, Wound Repair and Regeneration 19(2) (2011) 134-148.
[92] S. Pedron, A.M. Pritchard, G.A. Vincil, B. Andrade, S.C. Zimmerman, B.A. Harley, Patterning Three-Dimensional Hydrogel Microenvironments Using Hyperbranched Polyglycerols for Independent Control of Mesh Size and Stiffness, Biomacromolecules 18(4) (2017) 1393-1400.
[93] K.M. Schultz, K.A. Kyburz, K.S. Anseth, Measuring dynamic cell-material interactions and remodeling during 3D human mesenchymal stem cell migration in hydrogels, Proc Natl Acad Sci U S A 112(29) (2015) E3757-64.